PNAS Nexus, 2024, 3, pgae332
https://doi.org/10.1093/pnasnexus/pgae332
Advance access publication 8 August 2024
Research Report

Low-affinity LFA1-dependent outside-in signaling mediates avidity modulation via the Rabin8–Rab8 axis

Naoyuki Kondo [a,*], Yoshihiro Ueda [a] and Tatsuo Kinashi [a]

[a]Department of Molecular Genetics, Institute of Biomedical Science, Kansai Medical University, Hirakata, Osaka 573-1010, Japan
*To whom correspondence should be addressed: Email: kondonao@hirakata.kmu.ac.jp
Edited By Bruce Levine

Abstract

Lymphocyte interactions mediated by leukocyte integrin lymphocyte function–associated antigen 1 (LFA1) and intercellular adhesion molecules (ICAMs) are important for lymphocyte trafficking and antigen recognition. Integrins are regulated by the modulation of ligand-binding affinity and avidity (valency). Although the mechanism underlying high-affinity LFA1 binding has been investigated extensively, the molecular mechanisms by which low-affinity multivalent binding initiates adhesion remain unclear. We previously showed that ICAM1 and monoclonal antibodies that recognize specific LFA1 conformations induce the accumulation of LFA1 at the contact surface. In this study, we found that the small GTPase Rab8 is critical for intracellular transport and accumulation of LFA1 at cell contact areas mediated by low-affinity LFA1-dependent outside-in signaling. Super-resolution microscopy revealed that Rab8 co-localized with LFA1 in small vesicles near the contact membrane. Inactivation of Rab8 decreased ICAM1-dependent adhesion and substantially reduced LFA1 density on the contact membrane. The GTP-bound active form of Rab8 increased cell adhesiveness and promoted LFA1 accumulation at the contact area through co-trafficking with LFA1. Rab8 activation was induced by low-affinity conformation-dependent outside-in signaling via the guanine exchange factor Rabin8, which induced Rab8 activation at the cell contact area independent of Rap1. Single-molecule imaging of ICAM1 on a supported planner lipid bilayer demonstrated that Rab8 increased the frequency of LFA1–ICAM1 interactions without affecting their binding lifetime, indicating that Rab8 is mainly involved in the modulation of LFA1 avidity rather than LFA1 affinity. The present findings underscore the importance of low-affinity conformation-dependent outside-in signaling via the Rabin8–Rab8 axis leading to the initiation of LFA1 transport to the contact area.

Keywords: integrin activation, outside-in signaling, Rab8, Rabin8, single-molecule imaging

Significance Statement

Integrin adhesiveness is regulated by affinity and avidity. Increased affinity is driven by conformational changes of integrin from dominant inactive low-affinity conformations to active high-affinity conformations. The binding affinity of the integrin lymphocyte function–associated antigen 1 (LFA1) is controlled bidirectionally through intracellular signaling (inside-out signaling) and ligand binding (outside-in signaling). Although the importance of outside-in signaling mediated by high-affinity conformations in affinity and avidity modulation has been demonstrated, the significance of the low-affinity conformation remains unexplored. We identified a low-affinity LFA1-dependent signaling pathway in which outside-in signaling from low-affinity LFA1 activates the Rabin8–Rab8 axis to promote LFA1 accumulation at the adherent membrane, increasing cell adhesiveness via avidity modulation. We propose a new model of integrin activation by which low-affinity signaling initiates the activation cascade.

Introduction

The integrin lymphocyte function–associated antigen 1 (LFA1) is a heterodimeric transmembrane protein composed of the αL and β2 subunits, which play a critical role in lymphocyte trafficking, antigen recognition, and effector functions by binding to its counter-receptor intercellular adhesion molecules (ICAMs) (1). Integrin adhesiveness is generally low in resting lymphocytes and is regulated by affinity and avidity (valency). Affinity modulation is driven by dynamic conformational changes of the ectodomain of integrin: bent-closed (BC) conformations with low-affinity account for >99% of conformations (2), extended-closed (EC) conformations have intermediate affinity, and extended-open (EO) conformations have high affinity (Fig. 1A). LFA1 affinity is regulated in a bidirectional manner through intracellular signaling triggered by antigens and chemokines (inside-out signals) and ligand binding (outside-in signals). The transition from BC to EO conformations in LFA1 and very late activation antigen 5 increases ligand-binding affinity by more than several thousand-fold (3, 4). Avidity modulation is driven by surface clustering as well as the intracellular transport of integrins to the contact surface,

Competing Interest: The authors declare no competing interests.
Received: May 9, 2024. **Accepted:** July 30, 2024

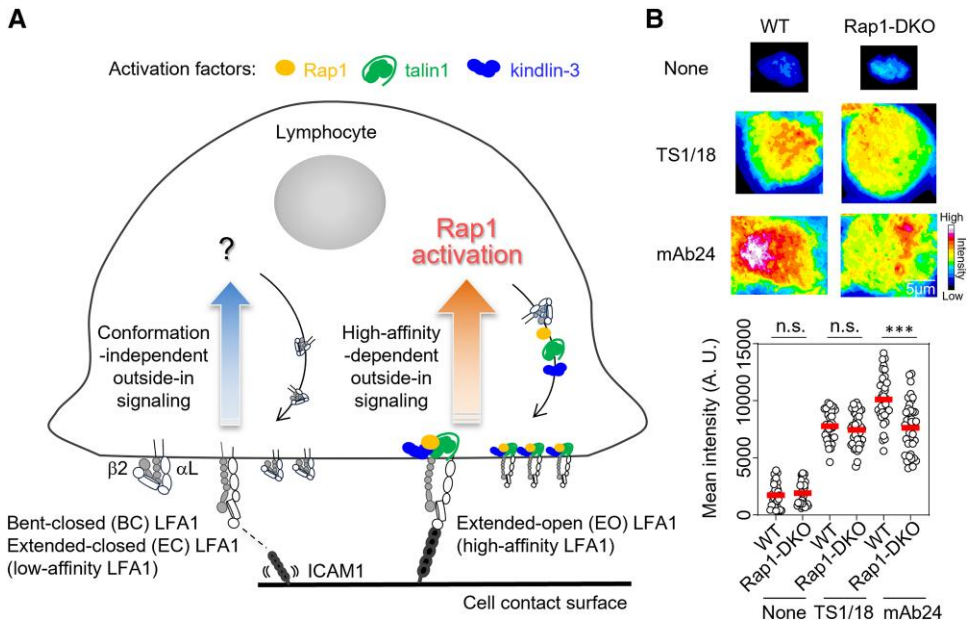

Fig. 1. Two distinct outside-in signaling pathways are involved in LFA1 activation. A) Schematic view of conformation-independent or high-affinity LFA1-dependent outside-in signaling. The pan-LFA1 antibody TS1/18 specifically induces LFA1 accumulation at adhesive membranes, independent of talin1 and kindlin-3 binding to LFA1. In contrast, mAb24, an antibody that specifically recognizes the EO LFA1 conformation inducing high-affinity LFA1–ICAM1 interactions, leads to potent LFA1 accumulation concomitant with talin1/kindlin-3 binding to LFA1 and Rap1 activation. B) Importance of Rap1 in the accumulation of LFA1 induced by different monoclonal antibodies. The mean intensity of LFA1 at the cell contact surface was measured by ImageJ. None: cells on PLL-coated dishes, WT ($n = 30$), Rap1a-KO and Rap1b-KO (Rap1-DKO; $n = 30$). TS1/18: cells on 15 μg/mL TS1/18-coated dishes, WT ($n = 34$), Rap1-DKO ($n = 42$). mAb24: cells on 15 μg/mL mAb24-coated dishes, WT ($n = 34$), Rap1-DKO ($n = 41$). A representative of two experiments is shown. Statistical significance was computed by Mann–Whitney test. n.s.: not significant. $^{***}P < 0.001$.

which enables multivalent binding of low-affinity integrins (5). Single-molecule imaging indicates that LFA1–ICAM1 interactions in immunological synapses (ISs) or in migrating T cells stimulated with chemokines are predominantly low-affinity interactions, with high-affinity interactions accounting for <10% (6). This suggests that multivalent low-affinity interactions and affinity modulation cooperatively sustain adhesion under physiological conditions.

The small GTPase Rap1 plays a central role in the bidirectional control of integrins; Rap1, which is activated by the T-cell receptor (TCR), chemokines, or phorbol 12-myristate 13-acetate (PMA), recruits the integrin adaptor proteins talin and kindlin-3 to the β2 cytoplasmic tails, leading to conformational changes and transient ICAM1 binding. Simultaneous engagement of ICAM1 and integrin adaptors induces and stabilizes the EO conformation, which in turn activates Rap1 to promote the recruitment of integrin adaptors and accumulation of LFA1 in the adherent membrane (1, 7). We previously reported the critical role of the Rap1-binding effector RAPL and downstream kinases, such as Mst1 and NDR1, in the bidirectional control of LFA1 (6, 8). Disruption of the RAPL–Mst1–NDR1 axis resulted in abnormal distribution of LFA1 and kindlin-3 as well as Rab family members and VPS4 in IS, implying that this pathway controls intracellular vesicular transport to mediate changes in LFA1 avidity (6).

In this study, we examined the molecular basis of LFA1 transport to the adherent membrane. To this end, we used ICAM1 or immobilized monoclonal antibodies against LFA1 to trigger outside-in signaling. We identified a Rap1-independent but Rab8-dependent process that was critically involved in adhesion, as deletion of Rab8 attenuated LFA1-mediated adhesion. In contrast, formation of the GTP-bound active form of Rab8 by Rabin8, a guanine exchange factor (GEF) of Rab8, enhanced cell adhesiveness. Outside-in signaling from LFA1 promoted Rab8 accumulation and Rab8-dependent LFA1 accumulation on the contact surface, indicating that Rab8 is critical for LFA1 transport to modulate avidity. We also demonstrated that outside-in signaling from low-affinity conformers of LFA1 activated the Rabin8–Rab8 axis. These results collectively indicate that the Rabin8–Rab8 axis regulated by LFA1 low-affinity conformers plays a key role in avidity modulation of LFA1.

Results

Existence of a Rap1-independent outside-in signaling pathway induced by pan-LFA1 antibody

We previously reported that high-affinity ligand binding by the LFA1 EO conformer or enforced induction of outside-in signaling by mAb24, a monoclonal antibody that specifically recognizes the EO conformation of the LFA1 β2 subunit, resulted in potent Rap1 activation, enhanced binding of the adaptors talin1 and kindlin-3 to LFA1, and LFA1 accumulation at the contact plane (Fig. 1A) (9). In contrast, induction of outside-in signaling by the pan-LFA1 β2 monoclonal antibody TS1/18, which recognizes all conformations of LFA1, resulted specifically in LFA1 accumulation (Fig. 1A) (9). The regulatory mechanisms underlying the dependence of these processes on different LFA1 conformations remain elusive.

We first aimed to determine the influence of Rap1 on the accumulation of LFA1 in response to LFA1 conformation-dependent outside-in signaling. Consistent with previous findings (9), TS1/18 stimulation promoted LFA1 accumulation, and mAb24 stimulation further increased it (Fig. 1B). Rap1 deletion had no impact on TS1/18-dependent LFA1 accumulation, but significantly

attenuated mAb24-dependent LFA1 accumulation (Fig. 1B). This observation suggests that while high-affinity LFA1-induced LFA1 accumulation relies on Rap1, conformation-independent LFA1 accumulation operates independently of Rap1. These findings suggest the possible existence of an alternative pathway for inducing LFA1 accumulation that is distinct from the Rap1 cascade.

Rab8 activation near the cell contact surface is important for lymphocyte cell adhesion

We previously showed that the membrane trafficking regulator Rab8 accumulates at the lymphocyte contact surface (6). Although Rab8 is present in the LFA1-containing vesicle fraction (10), the role of Rab8 in lymphocyte adhesiveness and LFA1 regulation remains unknown. Here, we focused on understanding the role of Rab8. We used the CRISPR/Cas9 technique to establish a lymphocyte cell line (BAF/LFA1) (9) with deletions in the Rab8a and Rab8b genes (Fig. 2A). We then isolated clones of wild-type (WT) and Rab8 double knockout (Rab8-DKO) lymphocytes exhibiting identical expression levels of LFA1 (Fig. 2B). Adhesion of Rab8-DKO cells to the ICAM1-coated glass surface was significantly decreased by ∼50% compared with that in WT cells (Fig. 2C). Rab8 function is regulated by cycling between a GTP-bound active form and a GDP-bound inactive form. To investigate the role of Rab8 activation status in adhesion, BAF/LFA1 cells were transfected with constitutively active (Q67L) and inactive (T22N) mutants of Rab8 (Figs. S1A and 2D). The Q62L mutant increased adhesiveness, whereas T22N inhibited it (Fig. 2D). Z-stack confocal images of GFP-fused Rab8 indicated that Rab8 accumulation at the cell contact area was not induced by inside-out stimulation by PMA, but rather by the co-existence of inside-out and outside-in signaling stimulated by ICAM1 + PMA, suggesting that outside-in signaling plays a key role in the accumulation of Rab8 at the contact area (Fig. 2E). To assess the density of LFA1 at the cell contact area, we used the phycoerythrin (PE)-conjugated non-blocking antibody TS2/4 and quantified the intensity by total internal reflection microscopy (TIRFM) (9). In the presence of ICAM1 + PMA, LFA1 density at the contact surface was lower in Rab8-DKO cells than in WT cells (Fig. 2F). To further determine the significance of Rab8 in outside-in signaling–regulated LFA1 accumulation, we measured the density after coating the contact surface with TS1/18 and mAb24. Intriguingly, we found that Rab8 not only regulated mAb24-induced LFA1 accumulation, but also affected TS1/18-induced accumulation (Fig. 2G). Collectively, these results highlight the pivotal role of Rab8 in modulating lymphocyte adhesion and LFA1 accumulation through conformation-independent outside-in signaling.

Regulation of LFA1 transport to the cell contact surface by Rab8

To track LFA1 dynamics during the adhesion process, we established a live-cell imaging system of LFA1 by introducing a photostable fluorescent dye via a SNAP-tag fused at the C-terminus of β2 (Fig. 3A). LFA1 was distributed uniformly at the contact surface (Fig. 3B, left), consistent with Figs. 2F. At the upper plane, LFA1 localized to the plasma membrane as well as the intracellular area in clusters of various sizes, namely, small dot-like clusters and large vesicle-like clusters (Fig. 3B, middle and right). Live imaging of LFA1 showed that some LFA1 clusters actively moved at the upper plane of the contact surface (Fig. 3C, Movie S1). Co-localization analysis using super-resolution microscopy demonstrated that Rab8 co-localized with LFA1 in relatively small clusters rather than in large vesicle-like clusters (Fig. 3D). Simultaneous live imaging of LFA1 and GFP-fused Rab8 showed co-trafficking of LFA1 with Rab8 in response to ICAM1-dependent cell adhesion (Fig. 3E, Movie S2). In Rab8-DKO cells, the size of some of the vesicular/cluster was larger than that in WT cells, but the number of small clusters was greater than that in WT cells (Fig. 3F). To characterize these intracellular clusters, we established cell expressing GFP-fused Rab5 or Rab11 (Fig. S2A and B), conventional markers for endosome (11), and visualized LFA1 with Rab5 and Rab11. Although Rab5 was not frequently co-localized with LFA1$^+$ clusters compared with Rab8 (Fig. 3G), Rab11 was co-localized with LFA1 more frequently than Rab8 (Fig. 3G). Rab8 deletion resulted in an increase in the co-localization of LFA1$^+$ clusters with both Rab5$^+$ and Rab11$^+$ vesicles compared with WT nearby the contact surface (Fig. 3G). We also quantified the frequency of the appearance of Rab11$^+$ vesicles nearby the contact surface and found that Rab8 deletion induced the accumulation of Rab11$^+$ vesicles compared with WT (Fig. 3G, β2/GFP-Rab11, Fig. S2C). Considering the existence of receptor recycling route from Rab5$^+$ early endosome to Rab11$^+$ recycling endosome in lymphocyte (12), these results suggest that Rab8 recruits LFA1 in part via Rab11$^+$ recycling endosomes derived from Rab5$^+$ early endosome to the plasma membrane at the cell contact surface.

Rabin8 functions upstream of Rab8 to control Rab8 activation at the contact surface under regulation of outside-in signaling from low-affinity LFA1

To understand the regulation of Rab8 activity at the cell contact plane, we investigated the effect of Rabin8, a GEF that recognizes Rab8 (13, 14). We first assessed the 3D localization of Rabin8 using GFP-fused Rabin8 (Fig. S3A) and found that Rabin8 localized to the cell contact surface in the presence of ICAM1 (Fig. 4A). Rabin8 knockout cells (Rabin8-KO, Fig. S3B and C) showed decreased LFA1-dependent lymphocyte adhesion (Fig. 4B) and LFA1 accumulation at the contact surface compared with WT cells (Fig. 4C), similar to the findings in Rab8-DKO cells (Fig. 2F).

Next, to assess the role of Rabin8 in the Rab8-mediated activation of the LFA1-dependent adhesion process, Rab8 activation was visualized using the affinity probe JFC1, which recognizes the GTP-bound active form of Rab8, fused with GFP (15) (Fig. S3D–F). GFP-JFC1 accumulated at the contact surface in response to TS1/18 stimulation and to a greater degree in response to mAb24 stimulation (Fig. 4D). The deletion of Rabin8 decreased the accumulation of active Rab8 (Fig. 4E and F), suggesting that outside-in signaling induces the activation of Rab8 in a Rabin8-dependent manner. Outside-in–dependent Rab8 activation and its dependence of Rabin8 were also verified by pull-down assay using GST-JFC1 (Fig. S3G).

To clarify the role of LFA1 conformation in Rab8 activation, we used BIRT377, a small molecule antagonist characterized by its ability to stabilize the low-affinity conformation of LFA1 (16, 17). The inhibitory effect of BIRT377 on LFA1-dependent adhesion was confirmed in BAF/LFA1 cells (Fig. S4A). The antibody against KIM127 recognizes the LFA1 EC conformation, whereas mAb24 recognizes the EO conformation (Fig. 1A). Although inside-out signaling by PMA induced a conformational change of LFA1 by exposing both the KIM127 and mAb24 epitopes (Fig. S4B) as reported previously (9), BIRT377 treatment increased KIM127 epitope exposure, but decreased mAb24 epitope exposure even in the presence of PMA, indicating that BIRT377 inhibits the transition of

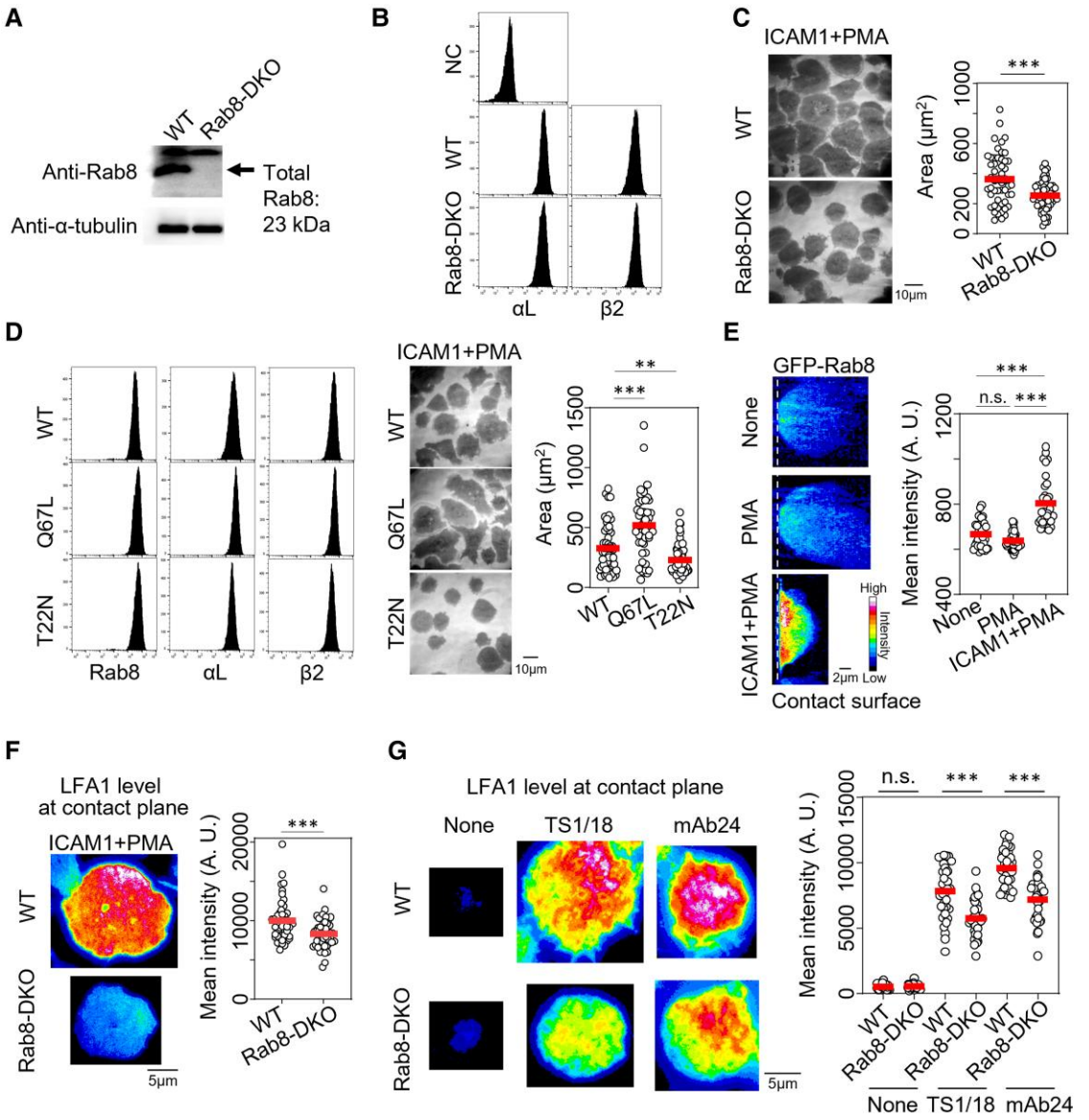

Fig. 2. GTP-bound active Rab8 is important for LFA1-dependent lymphocyte adhesion. A) Rab8 deletion verified by western blotting. B) Surface expression levels of αL and β2 in WT and Rab8-DKO cells. C) Adhesiveness of WT and Rab8-DKO cells to immobilized 3 μg/mL ICAM1 on capture antibody with inside-out 100 ng/mL PMA stimulation. WT ($n = 51$), Rab8-DKO ($n = 58$). D) Effect of the expression of Rab8 WT, active (Q67L), and inactive (T22N) forms tagged with GFP on cell adhesiveness under the condition in C). Left panels: expression levels of Rab8 mutants and LFA1. Right panels: comparison of adhesiveness between WT ($n = 49$) and mutants (Q67L: $n = 46$, T22N: $n = 62$). E) 3D projection images of GFP-Rab8 in cells showing the localization of GFP-Rab8 in response to inside-out (PMA, 100 ng/mL PMA) signaling and inside-out + outside-in signaling (ICAM1 + PMA, 3 μg/mL ICAM1 on capture antibody with 100 ng/mL PMA) compared with no stimulation (None, PLL-coated dish). Rab8 intensity at the cell contact surface (dotted line) was measured. None: $n = 36$, PMA: $n = 47$, ICAM1 + PMA: $n = 32$. F, G) LFA1 density at the cell contact surface. F) Effect of Rab8 deletion on the accumulation of LFA1 under the ICAM1 + PMA condition in E. WT ($n = 49$), Rab8-DKO ($n = 48$). G) Effect of Rab8 deletion on the accumulation of LFA1 in response to no stimulation (None, WT: $n = 44$, Rab8-DKO: $n = 38$), stimulation with 15 μg/mL TS1/18 (WT: $n = 35$, Rab8-DKO: $n = 40$), and 15 μg/mL mAb24 (WT: $n = 34$, Rab8-DKO: $n = 36$). A representative of more than two independent experiments is shown. Statistical significance was computed by Mann–Whitney test. $^{**}P < 0.01$, $^{***}P < 0.001$, n.s.: not significant.

LFA1 to the high-affinity EO conformation and maintains LFA1 in the low-/intermediate-affinity conformation. Subsequently, we measured the effect of BIRT377 on Rab8 activation and LFA1 density at the contact surface using TS1/18 and BIRT377. Remarkably, TS1/18-induced Rab8 activation (Fig. 4G) and LFA1 accumulation (Fig. S4C) occurred even in the presence of BIRT377 and at the same level as in the absence of BIRT377, and Rabin8 was required for this activation process (Fig. 4H and I). Of note, we previously demonstrated that KIM127 stimulation does not induce LFA1 accumulation (9), suggesting that low-affinity conformers play a major role in the BIRT377 + TS1/18-induced process. In addition, we further investigated the importance of Rap1 in Rabin8-KO cell under low-affinity conformer-dependent outside-in signaling. We established triple KO BAF/LFA1 (Rabin8-KO and Rap1-DKO, Fig. S4D and E) and found that both Rab8 activation and LFA1 accumulation were not further decreased by Rap1 deletion in Rabin8-KO (Fig. 4J and K), verifying that low-affinity conformer-dependent outside-in signaling is independent of Rap1 but dependent on Rabin8. Taken together, these findings support the existence of low-affinity LFA1-dependent outside-in signaling, which induces Rabin8-dependent Rab8 activation to enhance the accumulation of LFA1 at the contact surface.

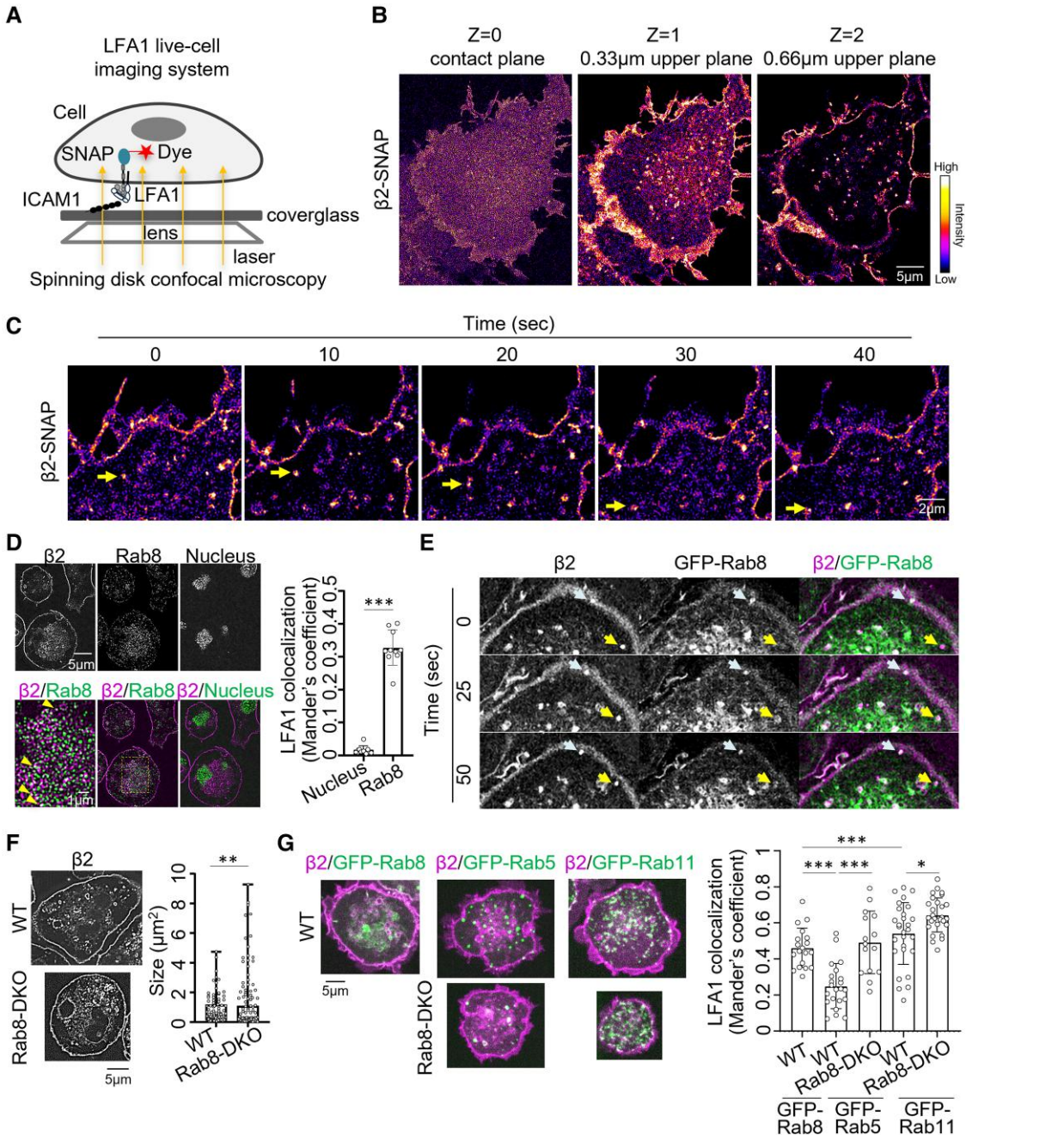

Fig. 3. Rab8 controls vesicular transport and sorting of LFA1. A) Schematic representation of the imaging system. BAF/LFA1 was adhered to immobilized 3 μg/mL ICAM1 on capture antibody with inside-out 100 ng/mL PMA stimulation. B) Distribution of LFA1 at the contact surface and upper neighborhood. LFA1 was visualized using SNAP-fused β2 (β2-SNAP) with 647-SiR dye and the SRRF imaging system. C) Time-lapse SRRF imaging of LFA1 clusters (arrows) moving in the intracellular space. D) Representative SRRF images of LFA1 (β2-SNAP), Rab8 stained by antibody, nucleus, and merged image. The enlarged image in the boxed area is shown in the lower left panel. The arrows indicate LFA1 clusters co-localized with Rab8. Co-localization of LFA1 (β2) with the nucleus or Rab8 was quantified using Mander's coefficient (mean ± SD, 10 cells from two independent experiments). E) Live-cell imaging of LFA1 (β2-SNAP) and Rab8 (GFP-Rab8). Arrows indicate LFA1 clusters co-trafficking with Rab8. F) Representative SRRF images of β2-SNAP in WT cells and Rab8-DKO cells. The sizes of clusters were quantified by Fiji and graphically presented by box and whisker plot. WT (97 clusters from 9 cells), Rab8-DKO (149 clusters from 8 cells). G) Co-localization of β2-SNAP with GFP-Rab5 or GFP-Rab11 nearby the contact surface in WT or Rab8-DKO cell. Co-localization of β2-SNAP with GFP-Rab8 was also shown for the comparison on the left. Statistical analysis was done as in D (mean ± SD, 19 cells [GFP-Rab8], 22 cells [GFP-Rab5], or 28 cells [GFP-Rab11] from two independent experiments). Statistical significance was computed by Mann–Whitney test. $^{*}P < 0.05$, $^{**}P < 0.01$. $^{***}P < 0.001$.

Rab8 is a specific regulator of LFA1 avidity

To elucidate the involvement of Rab8 in the regulation of affinity and avidity of LFA1, we performed single-molecule imaging analysis of ICAM1 on a supported planner lipid bilayer (SPLB), which was established previously (Fig. 5A) (6, 9). This analysis is used to investigate the binding frequency and binding time of the LFA1–ICAM1 interaction, which correspond to the avidity and affinity of LFA1, respectively. Rab8 deletion resulted in decreased trajectories of LFA1-bound ICAM1 (Fig. 5B). Statistical analyses of ICAM1 trajectories indicated that the binding frequency was

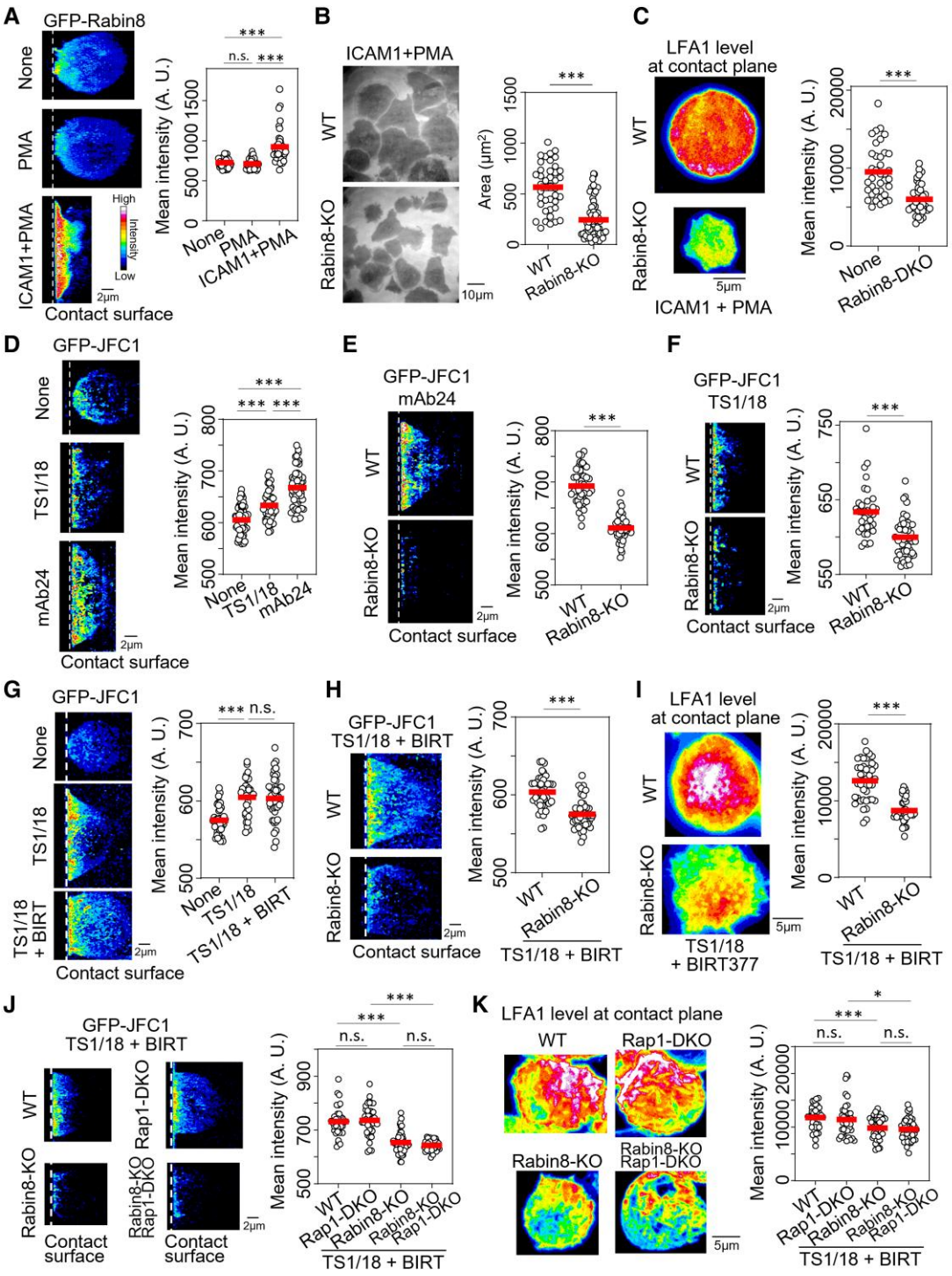

Fig. 4. Rabin8 activates Rab8 via low-affinity LFA1-mediated outside-in signaling. A) Accumulation of Rabin8 at the cell contact surface under the conditions in Fig. 2E. Representative 3D projection images of GFP-fused Rabin8 (GFP-Rabin8) are shown. The intensity of GFP-Rabin8 was measured at the contact surface (dotted line). None: $n = 39$, PMA: $n = 36$, ICAM1 + PMA: $n = 39$. B) Effect of Rabin8 deletion (Rabin8-KO) on LFA1-dependent lymphocyte adhesion under the conditions in Fig. 2C. WT: $n = 40$, Rabin8-KO: $n = 60$. C) Effect of Rabin8 deletion on LFA1 accumulation at the cell contact surface under the conditions in Fig. 2F. WT: $n = 37$, Rabin8-KO: $n = 38$. D–H) The detection of Rab8 activation at the contact surface using GFP-JFC1 as the reporter. Outside-in signaling was triggered by TS1/18 or mAb24 immobilized onto the contact surface (15 μg/mL each). The intensity of GFP-JFC1 at the contact surface was measured as the Rab8 activation level. D) None: $n = 60$, TS1/18: $n = 42$, mAb24: $n = 45$. E, F) Impact of Rabin8 deletion on Rab8 activation induced by mAb24 (E, WT: $n = 56$, Rabin8-KO: $n = 46$) and TS1/18 (F, WT: $n = 35$, Rabin8-KO: $n = 48$) determined using Rabin8-KO cells. G) Effect of 10 μM BIRT377, a low-affinity conformer stabilizing drug, on Rab8 activation triggered by TS1/18. None: $n = 41$, TS1/18: $n = 38$, TS1/18 + BIRT: $n = 47$. H) Effect of Rabin8 deletion on low-affinity conformer-dependent Rab8 activation. WT: $n = 41$, Rabin8-KO: $n = 47$. I) Effect of Rabin8 deletion on low-affinity conformer-dependent LFA1 accumulation at the contact plane. WT: $n = 41$, Rabin8-KO: $n = 43$. J) Effect of both Rap1 and Rabin8 deletion on low-affinity conformer-dependent Rab8 activation. WT: $n = 40$, Rap1-DKO: $n = 43$, Rabin8-KO: $n = 48$, Rap1 and Rabin8 triple knockout (Rabin8-KO Rap1-DKO): $n = 46$. K) Effect of both Rap1 and Rabin8 deletion on low-affinity conformer-dependent LFA1 accumulation at the contact plane. WT: $n = 38$, Rap1-DKO: $n = 40$, Rabin8-KO: $n = 44$, Rabin8-KO Rap1-DKO: $n = 43$. A representative of two independent experiments is shown. Statistical significance was computed by Mann–Whitney test. $^{*}P < 0.05$, $^{**}P < 0.01$, $^{***}P < 0.001$, n.s.: not significant.

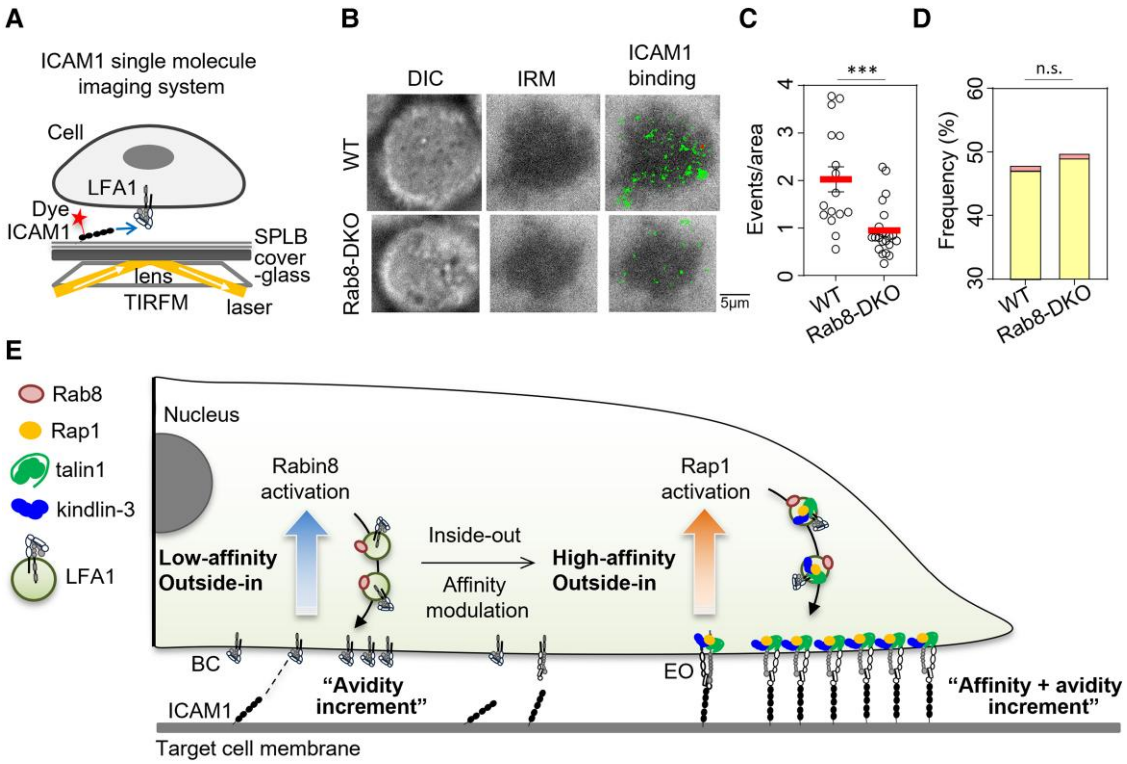

Fig. 5. Single-molecule imaging analysis was used to monitor the in vivo binding kinetics of ICAM1 to LFA1. A) A single-molecule imaging system of human ICAM1 using TIRFM. B) Trajectories of single-molecule hICAM1. Green trajectories: all trajectories. Red trajectories: trajectories with a binding time >10 s. The effect of Rab8 deletions on the frequency (C, WT: $n = 16$, Rab8-KO: $n = 22$) and the time (D, WT: $n = 1{,}429$, Rab8-KO: $n = 794$) of ICAM1 to LFA1 binding. A representative of two independent experiments is shown. The statistical significance of the frequency and the time was computed by Mann–Whitney test and χ^2 test, respectively. $^{***}P < 0.001$, n.s.: not significant. E) Model of LFA1 activation by low-affinity ligand binding and high-affinity ligand binding. The low-affinity outside-in signals increase LFA1 density at the contact surface via the Rabin8–Rab8 axis, which promotes high-affinity ligand binding associated with inside-out signaling, thereby strengthening outside-in signaling to facilitate adhesion.

significantly reduced compared with that in the WT (Fig. 5C), whereas binding time was not altered (Fig. 5D). These results suggest that Rab8 is a specific regulator of integrin binding frequency, so-called avidity.

Discussion

In this study, we demonstrated that Rab8 is critical for the intracellular transport and accumulation of LFA1 at the adherent membrane mediated by low-affinity LFA1-dependent outside-in signaling. The activation of Rab8 at the cell contact surface was controlled by Rabin8 and required for LFA1-dependent lymphocyte adhesion. Single-molecule imaging of the LFA1–ICAM1 interaction further revealed that Rab8 is involved in the modulation of the avidity rather than the affinity of LFA1. These findings collectively support the existence of a low-affinity conformation-dependent outside-in signaling pathway mediated by the Rabin8–Rab8 axis that is specifically important for the regulation of integrin avidity.

Previously, we found that outside-in signaling by high-affinity LFA1 conformers amplifies ligand binding of LFA1 via Rap1-dependent recruitment of LFA1 and integrin adaptors to stabilize transient cell adhesion (7, 9) (Fig. 1A). Although LFA1–ICAM1 interactions in lymphocytes are predominantly mediated by low-affinity binding (6), their precise functions are not fully understood. Bleijs et al. (18) described the physiological relevance of low-affinity ligand binding: binding of LFA1 to its low-affinity ligand ICAM3 facilitates the binding of LFA1 to ICAM1 and enhances LFA1–ICAM1-dependent adhesion, although the LFA1–ICAM3 interaction alone does not induce adequate adhesion. Li et al. (19) showed that low-affinity integrin conformers, including BC and EC, retain faster on-rate binding than high-affinity conformers. They proposed that fast integrin binding to its ligand may precede inside-out signaling to activate integrin. Our present study identified a novel role of low-affinity interactions between LFA1 and ICAM1 in avidity modulation of LFA1 mediated by vesicle transport. Unlike high-affinity interactions, the outside-in signals from low-affinity LFA1 did not require Rap1 activation. We propose a new model of outside-in triggered cell adhesion as follows (Fig. 5E): low-affinity LFA1-dependent outside-in signaling increases the density of LFA1 at the adherent membrane by mediating the transport of LFA1 through the Rabin8–Rab8 axis. The increase in LFA1 avidity and inside-out signaling-dependent affinity modulation cooperatively induce the bidirectional activation of LFA1 and promote high-affinity ligand binding to increase adhesiveness (9).

Rab8 regulates polarized transport/docking/fusion of proteins to the plasma membrane for the development of specialized organelles, such as during neurite outgrowth (20), primary cilium formation (21), and TCR recycling (22). Although the involvement of Rab11 and Rab27 in the regulation of LFA1 redistribution was reported previously (10, 23), the roles of Rab family proteins including Rab8 in avidity modulation of LFA1 have remained unclear. This study uncovered a novel function of Rab8 in the transport of LFA1 in part via recycling endosome to the cell contact surface mediated by low-affinity LFA1-dependent outside-in signaling, which is consistent with the role of Rab8 in polarized transport involved in specific cellular functions. Elucidating the

molecular mechanism underlying polarized LFA1 transport upon outside-in signaling in a pathophysiological setting would be important to improve our understanding of integrin-dependent lymphocyte regulation in health and disease.

Materials and methods

Reagents, plasmids, and viruses

Anti-CD11a (TS2/4), anti-CD18 (TS1/18), and anti-myc (9E10) antibodies were produced from hybridoma cells obtained from the American Type Culture Collection. Anti-SNAP antibody and SNAP-Cell 647 SiR were purchased from New England Biolabs. Anti-Rab8, anti-Rap1b, anti-rabbit IgG horseradish peroxidase (HRP)-linked, and antimouse IgG HRP-linked antibodies were from Cell Signaling Technology. Anti-GFP antibody for western blotting was from GeneTex. Anti-Rab3IP antibody was from Proteintech. Antimouse IgG-eFluor 660 was from eBioscience. PE-conjugated antihuman CD11a antibody was from BioLegend. Anti-α-tubulin antibody, PMA, and RPMI1640 culture medium were from Sigma-Aldrich. Anti-Rap1 antibody was from BD Biosciences. BIRT377 was from MedChemExpress. Glutathione beads were from GE Healthcare. Glass-bottom dishes with a diameter of 35 mm were from Matsunami. Rabbit antihuman IgG F(c) antibody was from Rockland.

Plasmids for Rap1a, Rap1b, Rab8a, Rab8b, and Rabin8 knockout were prepared, as described previously (9). Briefly, gRNAs specific for the target genes Rab8a (GTTCAAGCTGCTGCTGATCG), Rab8b (CTCATCGGCGACTCCGGCGT), and Rabin8 (CCGGTAGATGACGC TCGGGG and CTTCCGCTGTCGAGTGCGGA) were introduced into the pX458 plasmid. Rab8 mutation was introduced using the QuickChange method. Lentivirus production and infection for gene expression were performed, as described previously (9).

Biochemical analyses

Expression vectors for the proteins of interest were transfected into 293T cells using polyethyleneimine reagents, as described previously (6). Protein-containing lysates were prepared and analyzed by western blotting to detect the proteins of interest using specific antibodies.

Cell establishment and adhesion assay

Rab8a/b-DKO cells or Rabin8 knockout cells were generated from a Ba/F3 pro-B cell line deficient in mouse integrins β1, 2, 3, and 7 and with identical expression of human integrins αL and SNAP-fused integrin β2 (β2-SNAP) to that of parental cells (9) using CRISPR/Cas9 technology with the specific gRNAs described above. The surface expression of integrins was measured by flow cytometry. Target gene deletion in the established cells was verified by western blotting. For adhesion assays, cells (2×10^5) were seeded onto human ICAM1-Fc-coated dishes (3 μg/mL on 15 μg/mL antihuman IgG F(c) capture antibody) in the presence of 100 ng/mL PMA. Thirty minutes after application, differential interference contrast images and internal reflection microscopy (IRM) images were captured using an IX81 microscope (Evident). Cell adhesiveness was quantified by measuring the area of IRM. The mean and standard error of the quantified areas were compared.

Imaging of localization and trafficking by spinning disk microscopy

For co-localization assays, cells harboring β2-SNAP were stained with SNAP-Cell 647 SiR. Stained cells were adhered to ICAM1-coated dishes in the presence of 100 ng/mL PMA, and then fixed with 2% paraformaldehyde (PFA). Fixed cells were permeabilized with Triton X-100 and stained with the indicated antibodies. β2 and Rab8 co-localization was assessed using a Dragonfly spinning disk confocal microscope (Andor) with super-resolution radial fluctuation (SRRF)-stream technology (24). Mander's coefficient was calculated using Fiji (11). For the 3D localization assay, cells expressing the indicated reporter genes were placed in an ICAM1- or antibody-coated dish, fixed, and assessed using Dragonfly with Z-stack settings. For live-cell imaging, β2-SNAP was stained with the SNAP ligand, as described above. Stained cells were visualized using Dragonfly in a CO_2 chamber equipped with a humidifier at 37 °C. Two types of color channel, 647 SiR and GFP, were simultaneously monitored using the dual-camera setting.

Imaging using total IRM

To measure the level of LFA1 at the contact plane, cells were stained for αL integrin using nonblocking TS2/4 antibody conjugated with PE for 10 min at 37 °C followed by one wash with medium. Stained cells were placed onto a glass-bottom dish coated with ICAM1, monoclonal antibodies, or poly-lysine (PLL), incubated for 30 min at 37 °C, and fixed with 2% PFA. The level of LFA1 at the contact plane was monitored using TIRFM (Evident) (9). The average fluorescence intensity at the cell contact area was quantified by ImageJ, and statistical analysis was performed with Prism 10 (GraphPad Software Inc.).

Single-molecule measurements

The single-molecule dynamics of ICAM1 was measured using methods described previously (6, 9). Briefly, ATTO 647N-labeled human ICAM1-GPI in liposomes was incorporated into an SPLB consisting of 0.4 mM 1,2-dioleoyl-*sn*-glycero-3-phosphocholine and imaged using TIRFM. Single particle tracking and statistical analyses of ICAM1 were also performed, as described previously (6, 9).

Statistical analysis

Mean values, Mann–Whitney test, and χ^2 test were calculated using GraphPad Prism software.

Acknowledgments

The authors thank R. Hamaguchi for her excellent technical support, Y. Kamioka and Y. Mimori-Kiyosue for their helpful discussions, and M. Fukuda for his kind provision of GFP-fused Rab plasmids.

Supplementary Material

Supplementary material is available at *PNAS Nexus* online.

Funding

This study was supported by JSPS KAKENHI (JP20K07331; to N.K.), (JP22H02623; to T.K.), the Takeda Science Foundation, and the Strategic Project for Proofreading and Submission Support of International Academic Papers by Kansai Medical University.

Author Contributions

N.K. and T.K. conceived the experiments. N.K. designed the experiments, and performed the experiments and analyses. N.K., Y.U., and T.K. wrote the manuscript.

Data Availability

The source data for Figs. 1–5 are deposited in Zenodo with DOI: 10.5281/zenodo.13180048.

References

1 Kondo N, Ueda Y, Kinashi T. 2022. LFA1 activation: insights from a single-molecule approach. *Cells*. 11:1751.
2 Li J, *et al.* 2017. Conformational equilibria and intrinsic affinities define integrin activation. *EMBO J*. 36:629–645.
3 Li J, Springer TA. 2017. Energy landscape differences among integrins establish the framework for understanding activation. *J Cell Biol*. 217:397–412.
4 Shimaoka M, *et al.* 2006. AL-57, a ligand-mimetic antibody to integrin LFA-1, reveals chemokine-induced affinity up-regulation in lymphocytes. *Proc Natl Acad Sci U S A*. 103:13991–13996.
5 Carman CV, Springer TA. 2003. Integrin avidity regulation: are changes in affinity and conformation underemphasized? *Curr Opin Cell Biol*. 15:547–556.
6 Kondo N, *et al.* 2017. NDR1-dependent regulation of kindlin-3 controls high-affinity LFA-1 binding and immune synapse organization. *Mol Cell Biol*. 37:e00424-16.
7 Kamioka Y, *et al.* 2023. Distinct bidirectional regulation of LFA1 and alpha4beta7 by Rap1 and integrin adaptors in T cells under shear flow. *Cell Rep*. 42:112580.
8 Katagiri K, Imamura M, Kinashi T. 2006. Spatiotemporal regulation of the kinase Mst1 by binding protein RAPL is critical for lymphocyte polarity and adhesion. *Nat Immunol*. 7: 919–928.
9 Kondo N, Ueda Y, Kinashi T. 2021. Kindlin-3 disrupts an intersubunit association in the integrin LFA1 to trigger positive feedback activation by Rap1 and talin1. *Sci Signal*. 14:eabf2184.
10 Capece T, *et al.* 2017. A novel intracellular pool of LFA-1 is critical for asymmetric CD8(+) T cell activation and differentiation. *J Cell Biol*. 216:3817–3829.
11 Finetti F, *et al.* 2014. Specific recycling receptors are targeted to the immune synapse by the intraflagellar transport system. *J Cell Sci*. 127:1924–1937.
12 Onnis A, Finetti F, Baldari CT. 2016. Vesicular trafficking to the immune synapse: how to assemble receptor-tailored pathways from a basic building set. *Front Immunol*. 7:50.
13 Hattula K, Furuhjelm J, Arffman A, Peranen J. 2002. A Rab8-specific GDP/GTP exchange factor is involved in actin remodeling and polarized membrane transport. *Mol Biol Cell*. 13: 3268–3280.
14 Blumer J, *et al.* 2013. RabGEFs are a major determinant for specific Rab membrane targeting. *J Cell Biol*. 200:287–300.
15 Hattula K, *et al.* 2006. Characterization of the Rab8-specific membrane traffic route linked to protrusion formation. *J Cell Sci*. 119: 4866–4877.
16 Schürpf T, Springer TA. 2011. Regulation of integrin affinity on cell surfaces. *EMBO J*. 30:4712–4727.
17 Moore TI, Aaron J, Chew TL, Springer TA. 2018. Measuring integrin conformational change on the cell surface with super-resolution microscopy. *Cell Rep*. 22:1903–1912.
18 Bleijs DA, Binnerts ME, van Vliet SJ, Figdor CG, van Kooyk Y. 2000. Low-affinity LFA-1/ICAM-3 interactions augment LFA-1/ICAM-1-mediated T cell adhesion and signaling by redistribution of LFA-1. *J Cell Sci*. 113(Pt 3):391–400.
19 Li J, Yan J, Springer TA. 2021. Low-affinity integrin states have faster ligand-binding kinetics than the high-affinity state. *Elife*. 10:e73359.
20 Homma Y, Fukuda M. 2016. Rabin8 regulates neurite outgrowth in both GEF activity-dependent and -independent manners. *Mol Biol Cell*. 27:2107–2118.
21 Nachury MV, *et al.* 2007. A core complex of BBS proteins cooperates with the GTPase Rab8 to promote ciliary membrane biogenesis. *Cell*. 129:1201–1213.
22 Finetti F, *et al.* 2015. The small GTPase Rab8 interacts with VAMP-3 to regulate the delivery of recycling T-cell receptors to the immune synapse. *J Cell Sci*. 128:2541–2552.
23 Samuelsson M, *et al.* 2017. Rhob controls the Rab11-mediated recycling and surface reappearance of LFA-1 in migrating T lymphocytes. *Sci Signal*. 10:eaai8629.
24 Gustafsson N, *et al.* 2016. Fast live-cell conventional fluorophore nanoscopy with ImageJ through super-resolution radial fluctuations. *Nat Commun*. 7:12471.